Airplane motors employing superconducting DC field windings and conventional conductor AC windings

S S Kalsi[1], J G Storey[2], G Lumsden[2] and R A Badcock[2]

[1] Kalsi Green Power Systems, LLC, Princeton, New Jersey, 08540 USA
[2] Paihau - Robinson Research Institute, Victoria University of Wellington, Lower Hutt, 5010 New Zealand

Email: rod.badcock@vuw.ac.nz

Abstract. Many organizations are developing compact lightweight highly efficient rotating machines for airplane applications. These machines include permanent magnets for excitation and an iron-core with and without superconducting windings. Air-core (no magnetic iron) machines have the potential to be the most lightweight and efficient. Such machines can use superconductors for both DC excitation field coils and AC armature coils, which need conductors under development, like MgB_2 and Bi2212. If liquid-hydrogen (LH_2) is available on a plane and can be used as a coolant, it becomes feasible to develop machines with AC armature coils made from conventional conductors like copper, aluminium, and high-conductivity aluminium.

This paper describes conceptual designs for a 3 MW, 4,500 RPM motor employing REBCO CORC conductor for the DC field coils and conventional conductor Litz cable for the AC armature coils cooled by LH_2 available on the plane. Both rotor and stator coils are contained in separate cryostats. The DC excitation coils on the rotor are operated at 40 K to work successfully with a brushless flux pump exciter. Likewise, stator AC coils are cooled with available LH_2 to take advantage of the lower resistivity of conventional conductors at cryogenic temperatures. Motor size, mass and losses are compared for stator windings employing copper, aluminium, and high-conductivity aluminium (Hyper-Al). Compared with copper and aluminium machines, the machine employing Hyper-Al has smaller size, mass and total losses.

1. Introduction

Single-aisle airplanes are being considered for all-electric propulsion to reduce greenhouse gas (GHG) emissions. To achieve these goals, electric motors with attributes of high volumetric power, high power density and high efficiency are desired [1]. Currently, a wide variety of motor concepts [2,3,4,5,6] are being considered. Motors employing high-temperature superconductors (HTS) are being viewed as an enabling technology to achieve these goals [7,8]. If LH_2 is available on a future airplane, the option of using conventional AC armature windings becomes attractive, especially if the high-conductivity aluminum (Hyper-Al) [9] becomes available in desired wire form. Using a conventional conductor winding for the armature also eliminates the risk of superconductor quench issues associated with Bi2212 and MgB_2 windings. This paper presents concept designs for 3 motors using armature (stator) windings made of Hyper-Al, aluminum, and copper. For a target motor rating of 3 MW, 4500 RPM three topologies are compared for size, mass and efficiency.

2. Propulsion Motor Concepts

Design specifications for a 3 MW, 4500 RPM motor provided in Table 1 are selected based on the NASA recommendations [10]. Only 4-pole motors are used in this study as being close to optimum for achieving minimum size and mass attributes essential in an airplane motor. The field winding on the rotor uses REBCO coils operating at 40 K and the armature coils on the stator operate at a nominal 20 K cooled using LH_2.

Table 1 Specifications for a 3 MW, 4500-RPM Aircraft Propulsion Motors

MACHINE SPECIFICATIONS	Value
Rating, MW	3
Power factor	0.98
Number of phases	3
Desired DC voltage, V-rms	1000
Number of poles	4
Rated rotational speed, RPM	4500
Rated frequency, Hz	150
Ambient coolant temp., K	300
Rotor operating temp., K	40
Stator operating temp., K	20
EM Shield operating temp., K	40

An analytical model based on reference [11] is utilized for comparative evaluation of the three motor concepts. The motors selected for evaluation are designed with the following assumptions.

a) REBCO CORC windings for field excitation coils operating at 40 K.
b) Litz cable made of selected conductor stator windings cooled using LH_2 at 20 K.
c) Air-core design - no magnetic iron within the magnetic circuit.
d) Stator winding designed for <1000 V.
e) EM shield implemented in the shroud of the ducted propulsion fan to control stray field.

3. Propulsion Motor Concepts

Three synchronous motors are compared in the concept design with the following stator windings: Hyper-Al, Aluminium and Copper

The most important characteristic of these conductors is their resistivity at the operating temperature. Figure 1 shows a resistivity comparison between 10 K and 50 K. Below 30 K, the resistivity of Hyper-Al is significantly lower than aluminum and copper. The resistivity of Hyper-Al is based on a paper by AFRL [9]. At the operating temperature of 20-25 K, the resistivities of aluminum and copper are almost identical. Thus, from a resistivity point of view, aluminum is preferable over copper at very low temperatures.

3.1. Synchronous Motor Concept

Figure 2 shows an AC synchronous motor with an HTS field winding. The HTS field coils attached to the rotor create a rotating magnetic field experienced by the stationary armature winding. A superconducting machine can produce much larger airgap magnetic field than a conventional copper wound machine. Since this field is typically above the ferromagnetic saturation field an air-core is used, i.e. no ferromagnetic material is in the rotor or stator. The armature winding is constructed using non-metallic materials like G10 teeth. The stator winding is constructed using Litz cable supported in a non-metallic mechanical structure. Each stator coil uses a rectangular Litz cable available commercially with one change (Figure 3). Each strand is made of round Litz cable having many smaller diameter sub-strands. The selected strand diameter is the same as for the commercial copper cables, but the copper is replaced with Hyper-Al or aluminum. Any manufacturability issues relating to non-copper materials are left for future studies.

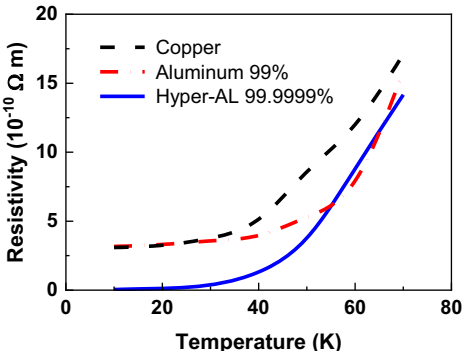

Figure 1 Resistivity of Hyper-Al, Aluminum and Copper in magnetic field of 0.65 T versus temperature.

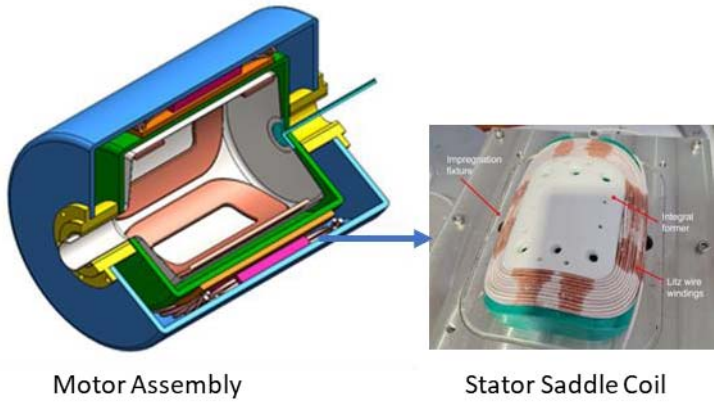

Figure 2 . Conceptual configuration of a superconducting synchronous motor (left) featuring saddle-shaped coils (right).

3.2. Magnetic Analysis

The selected concept for the airplane motor for this study is based on an air-core topology. The motor designs are based on analytical models [11]. The stator windings generate fundamental and harmonic fields of odd order in the airgap. Under steady-state operation, the rotor spins synchronously with the rotating fundamental field created by the three-phase armature currents, and the field winding experiences it only as a DC magnetic field. However, the harmonic fields not synchronous with the rotor induce varying currents in the rotor components causing heating and efficiency loss.

The very low resistivity (or high conductivity) of Hyper-Al becomes a concern for high eddy-current loss in the strands. This requires judicial choice of strand diameter. Figure 4 shows I^2R and eddy-current losses as a function of RRR (ratio of resistivities at room temperature to low operating temperature). At low temperatures, the resistivity of materials is also influenced by magnetic fields. The RRR value has been corrected for the operating field and temperature as per Sumption [12]. At low values of RRR, I^2R loss dominates with low eddy-current loss while the total loss (sum of I^2R and eddy-current) is high. At larger values of RRR, eddy-current loss becomes larger than I^2R loss. The total loss is minimum when I^2R and eddy-current losses are equal. In the motor designs discussed later this occurs when RRR is 740.

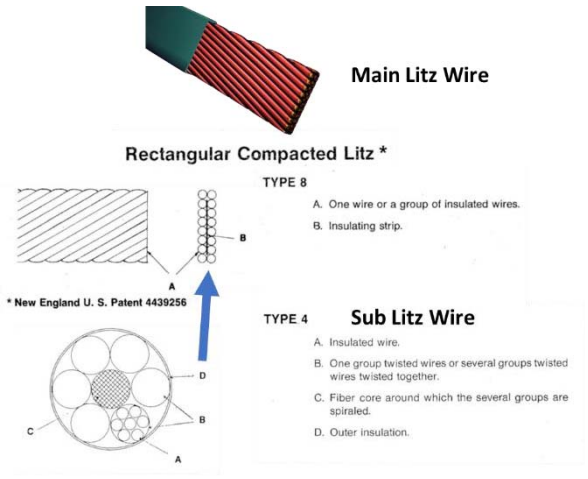

Figure 3 Selected Litz wire configuration for stator coils from New England Wire Catalog.

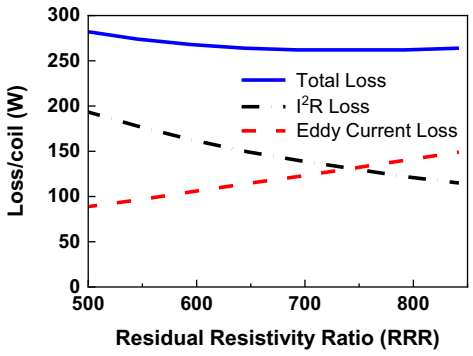

Figure 4 Comparison of I^2R and Eddy-current losses in stator coils made of Hyper-Al.

Table 2 Field distribution due to rotor and stator windings

Rotor Field Harmonics in stator (%)	**Hyper-Al**	**Aluminium**	**Copper**
- Fundamental Harmonic	100	100	100
- 3rd Harmonic	0.00	0.00	0.00
- 5th Harmonic	-9.49	-12.55	-12.55
- 7th Harmonic	0.48	0.73	0.73
Stator Field Harmonics at rotor EM shield (%)			
Fundamental	100	100	100
3rd Harmonic	113	105	105
5th Harmonic	17.9	15.6	15.6
7th Harmonic	4.8	3.9	3.9
Stator harmonic fields at HTS Field Winding			
5th Harmonic Radial field (T)	5.68E-06	3.69E-06	3.69E-06
5th Harmonic Tangential field (T)	-5.68E-06	-3.69E-06	-3.69E-06
7th Harmonic Radial field (T)	8.27E-07	5.62E-07	5.62E-07
7th Harmonic Tangential field (T)	-8.27E-07	-5.62E-07	-5.62E-07

Magnetic field distributions due to rotor and stator windings are shown in Table 2. By judicial distribution of the field winding turns the 3rd harmonic fields experienced by the stator winding are essentially eliminated. The only significant harmonic component is the 5th (9.5% of fundamental for the Hyper-Al coils.) This component is larger for Aluminum and Copper coils but is tolerable as the additional eddy-current loss is insignificant. Higher harmonics (7th and higher) are not problematic.

Table 3 Configurational details for three synchronous motors.

MECHANICAL DIMENSIONS	Hyper-Al	Aluminium	Copper
Thickness of torque tube, mm	2	2	2
Torque tube outside radius, mm	143	173	173
Torque axial length, mm	400	400	400
Field winding inside radius (R1), mm	130	160	160
Field winding outside radius (R2), mm	138	168	168
Field winding pack span angle-min (alpha), deg	18	18	18
Field winding pack span angle-max (beta), deg	42	42	42
Active axial length of coils (Lact), mm	400	400	400
Inside radius of EM shield (Rs1), mm	153	183	183
Outside radius of EM shield (Rs2), mm	160	190	190
Radial gap between rotor and stator windings (airgap), mm	5	5	5
Stator coil dimensions			
Inside radius of stator winding (R3), mm	165	195	195
Mean radius of stator winding (R34), mm	170	206	206
Outside radius of stator winding (R4), mm	174	216	216
Inside radius of stator winding (R5), mm	177	222	222
Mean radius of stator winding (R56), mm	181	232	232
Outside radius of stator winding (R6), mm	186	243	243
Cryostat space between stator coils and RT case (tcs), mm	25	25	25
Wall thickness of case (tsc), mm	10	10	10

Currents in the stator winding generate harmonics experienced by the rotor components. Table 2 also lists stator harmonics as percent of the fundamental experienced at the outer surface made of AL6061-T6. The high magnitude of the 3rd harmonic is not problematic as the sum of 3-phase fields sums to zero. Other harmonics are a much smaller fraction of the fundamental and are attenuated to the micro-tesla level as experienced by the field winding (see Table 2). Any AC loss in the HTS rotor coils is insignificant.

The switched-mode power electronics driving the AC stator windings also create undesirable time harmonic current pulses. Magnetic fields produced by these harmonics cause AC losses on the rotor components. The eddy-current heating due to these harmonic components is absorbed by the rotor EM shield. A second, larger EM shield, is also included outside the stator, for protecting the environment from stray EM-field effects. In airplane applications, the shroud of the ducted fans serves as the external EM shield.

The HTS field winding on the rotor is cooled by a cooler integrated within the shaft [13]. The cooling system maintains the field windings at 40 K by circulating gas through cooling channels located inside the windings. Since a turboelectric aircraft may be fueled with LH_2, the cryogenic gas is suggested to be cooled by the LH_2, and a separate refrigeration system might not be necessary. None-the-less efficiency and mass are reported including the refrigeration system.

3.3. Synchronous Motor Design

The synchronous motor parameters and dimensions are summarized in Table 3. The excitation field winding located on the rotor lies within radii R1 and R2. It is supported against radial forces by a suitable mechanical structure. The field winding is constructed using CORC cable made with 2 mm wide REBCO conductor. A 7 mm thick aluminum 6061-T6 cylinder forming the outer wall of the rotor cryostat intercepts AC harmonic fields from the stator. Details for the CORC cable made of 2 mm wide REBCO tapes are summarized in Table 4. A clear 5 mm airgap separates rotor and stator. The stator coils are constructed using Litz cable cooled to 20 K using LH2 as the coolant source. The stator winding has 6 coils, 3 are located within radii R3 and R4 and the other 3 within radii R5 and R6. The stator coils are supported in a non-metallic structure. The stator coils operating at 20 K are thermally

isolated from the motor case with cryostat wall thickness of ~25 mm. The shroud of the ducted propulsion fan located at radius > 1 m serves as an environmental magnetic shield.

Table 4 Configuration of REBCO CORC cable for field coils.

CORC Parameters-ROTOR	Hyper-Al	Aluminium	Copper
- Width of tapes, mm	2	2	2
- Number of layers	12	12	12
- Number of tapes	30	30	30
- Tape pitch, mm	6	6	6
- Cable OD, mm	3.7	3.7	3.7
- Cable I_c, kA	5.6	5.5	5.5
- Cable core material, Cu=0, Al=1	1	1	1
- Cable mass, kg/m	0.068	0.068	0.068

4. Performance Comparison of HTS Motors

Table 5 compares terminal parameters of the three motors. All motors are sized for a propulsion power of 3.2 MW at 4500 RPM. The RMS line voltage is 1 kV for the Hyper-AL motor and 1.6 kV for the other two. The stator winding could be powered as a single 3-phase winding or 2-Y 3-phase split windings by connecting 3 coils in each stator winding layer to form a Y-winding. However, if a motor voltage higher than 1 kV is not acceptable, then each coil could be powered individually. In this case, the coil voltage for the Hyper-AL motor would be 0.71 kV (peak) and 1.11 kV (peak) for Aluminum and Copper motors. Field winding current for all motors is about 4.2 kA, which is acceptable for the flux pump located on the rotor.

Table 5 Terminal Parameters for 3 motors

TERMINAL PARAMETERS	Hyper-Al	Aluminium	Copper
Machine Apparent Power, MVA	3.31	3.27	3.27
Machine Real Power, MVA	3.24	3.21	3.21
Phase voltage, kV_rms	1.00	1.57	1.57
Peak phase voltage, kV	1.42	2.22	2.22
2-Y Split Peak line voltage, kV	1.23	1.92	1.92
Phase current, A	1,100	697	697
Field excitation current, A	4,191	4,274	4,274
Load angle at rated load, deg	22.6	13.8	13.8
Stator Coil voltage, kV_peak	0.71	1.11	1.11
Stator Coil current, A_peak	1,556	985	985

The performance parameters are summarized in Table 6. Synchronous reactance for the Hyper-Al motor is nearly twice that of the other motors. This is due to the very small radial build of this motor (R6-R3 = 21 mm) versus 48 mm for others. Transient and sub-transient reactance are important for controlling currents due to power electronic generated harmonic voltages. The field winding time constant is large for all machines. This implies that in event of a fault, the winding current will persist for a long time, and it would be necessary to discharge field coils quickly to prevent damage to the winding. However, the sub-transient time constants are quite small implying that currents due to flux trapped in the rotor EM shield decay very rapidly.

The losses and efficiency for all motors are summarized in Table 7. Losses on the rotor and stator are listed separately. Dominant loss on the rotor is associated with the flux pump exciter. This loss component includes I^2R loss in 5 joints (3 between the 4 coils and 2 at the flux pump). The joint loss is estimated using an assumed joint resistance of 1 micro-ohm. Stator winding losses are calculated using a winding temperature of 25 K (5 K higher than nominal 20 K). The stator winding loss for the Hyper-Al winding is only about ½ of the Aluminum and Copper windings. About 10% of this loss is assigned

for pumping coolant to the windings. PWM losses are assumed zero as it is believed that a pure sinusoidal current could be supplied to the stator.

Table 6 Performance parameters for all motors.

PERFORMANCE PARAMETERS	Hyper-Al	Aluminium	Copper
Base voltage/phase, V_rms	1,003	1,567	1,567
Base current, A_rms	1,100	697	697
Per-unit base impedance, Ohm	0.91	2.25	2.25
D-axis Synchronous reactance - Xd, pu	0.46	0.26	0.26
D-axis Transient reactance - Xd', pu	0.34	0.20	0.20
D-axis Sub-transient reactance - Xd", pu	0.33	0.20	0.20
Q-axis Synchronous reactance - Xq, pu	0.46	0.26	0.26
Q-axis Sub-transient reactance - Xq", pu	0.37	0.22	0.22
Armature short-circuit time constant, s	1.57	0.42	0.42
D-axis transient time constant, s	321	513	513
D-axis sub-transient time constant, s	0.07	0.03	0.03
Field winding time constant, s	442	683	683
Q-axis sub-transient time constant, s	0.11	0.08	0.08
Zero sequence impedance, s	0.10	0.15	0.15

In the efficiency calculations, power consumption by the cryocooler is included as a loss. If LH_2 is available for free, the efficiency of Hyper-Al motor is about 0.1% higher than the other two motors. Conduction through torque tube is small compared to other loads (0.02-0.03 W).

Table 7 Motor losses and efficiency.

ROTOR LOSS SUMMARY	Hyper-Al	Aluminium	Copper
Conduction through torque tube, W	0.03	0.02	0.02
Radiation load, W	3.4	4.7	4.7
Flux pump, W	43.9	45.7	45.7
REBCO conduction, W	0.7	1.5	1.5
Rotor EM Shield, W	0.2	0.3	0.3
Field winding AC losses, W	1.3	1.1	1.1
Total losses on rotor, W	49.53	53.32	53.32
STATOR LOSS SUMMARY	**Hyper-Al**	**Aluminium**	**Copper**
I^2R loss, W	1,843	3,601	3,600
Stator cooler power, W	184	360	360
PWM Switching Losses, W	0	0	0
Total stator losses, W	2,027	3,961	3,960
Stator cooling heat flux, W/cm^2	0.71	0.76	0.76
EFFICIENCY CALCULATIONS	**Hyper-Al**	**Aluminium**	**Copper**
Cryocooler power for rotor, kW	1.9	2.1	2.1
Cryocooler power for stator, kW	0.1	0.2	0.2
Friction losses, kW	0.3	0.3	0.3
Total losses, kW	4.2	6.5	6.5
Efficiency at rated load, %	99.9	99.8	99.8

Table 8 summarizes reasonable mass estimates for each motor, including the mass of the refrigeration system. The environmental EM shield mass is not included as this function is served by the ducted fan shroud already expected to be present on the aircraft. Current leads for the HTS windings are also excluded in favor of employing an HTS dynamo [14] that is expected to reduce both the mass of the current supply path, and the total heat conduction into the cryogenic environment of the rotor coils. Practical implementations of these devices have shown the potential to deliver kA currents within HTS coils without adding a significant heat leak [15]. Masses reported in the table should be used for relative

comparison among options, more precise mass estimates would require a detailed design analysis. Thermal conduction through torque tube is small compared to other loads.

Motor masses have been estimated by assigning mass to various structural and winding components. On the rotor the EM shield (made of Al6061-T6) and field winding masses are comparable. On the stator side, the motor casing is the dominant mass for the Hyper-Al motor, but the winding mass dominates the other motors. The total mass of the Hyper-Al motor is about half of the other motors. The power density of the Hyper-Al motor is ~ 38 kW/kg, which looks attractive for airplane applications.

Table 8 Summary of Motor component mass (kg).

ROTOR MASS SUMMARY	**Hyper-Al**	**Aluminium**	**Copper**
Shaft, kg	1.8	1.9	1.9
Torque tube, kg	1.2	1.5	1.5
Field winding, kg	19.9	25.7	25.7
EM shield, kg	21.9	27.8	27.8
Rotor end flanges, kg	0.9	1.2	1.2
Flux pump, kg	4.7	7.0	7.0
Bearings, kg	0.2	0.2	0.2
Total weight of rotor, kg	**50.6**	**65.4**	**65.4**
STATOR MASS SUMMARY	**Hyper-Al**	**Aluminium**	**Copper**
Stator winding, kg	3.6	53.3	53.3
Torque tube, kg	2.7	3.8	3.8
Machine case, kg	14.8	20.3	20.3
EM shield, kg	0.0	0.0	0.0
Machine end-flanges, kg	4.6	7.5	7.5
Misc. Fittings, kg	3.9	5.6	5.6
Total stator weight, kg	**29.5**	**90.5**	**90.5**
TOTAL MASS SUMARY	**Hyper-Al**	**Aluminium**	**Copper**
Total rotor weight, kg	50.6	65.4	65.4
Total stator weight, kg	29.5	90.5	90.5
Weight of motor alone, kg	**80.1**	**155.8**	**155.8**
Weight of cryocooler, kg	3.3	3.6	3.6
Power density, without cryocooler, kW/kg	***38.6***	***19.6***	***19.6***

5. Performance Comparison of HTS Motors

Three superconducting synchronous motor options are compared in this paper using Hyper-Al, Aluminum and Copper stator coils. The Hyper-Al motor looks attractive compared to the other two motors. The power density (38 kW/kg) of the Hyper-Al motor looks quite competitive with an all-superconducting motor without concerns for stability of superconductor employed in the stator coils. This study concludes that the Hyper-Al motor should be studied more thoroughly and that solutions should be identified for the procurement (and cost) of Hyper-Al wire. Of course, a full materials evaluation covering cyclic behavior, long term degradation and other materials properties will need to be investigated before a machine is committed.

6. Conclusions

Three superconducting synchronous motor options are compared in this paper using Hyper-Al, Aluminum and Copper stator coils. The Hyper-Al motor looks attractive compared to the other two motors. The power density (38 kW/kg) of the Hyper-Al motor looks quite competitive with an all-superconducting motor without concerns for stability of superconductor employed in the stator coils. This study concludes that the Hyper-Al motor should be studied more thoroughly and that solutions should be identified for the procurement (and cost) of Hyper-Al wire. Of course, a full materials evaluation covering cyclic behavior, long term degradation and other materials properties will need to be investigated before a machine is committed.

7. References

[1] Collier, F. and Wahls, R. , "NASA ARMD Strategic Thrust 3: Ultra-Efficient Commercial Vehicles Subsonic Transport," ed. Presented at Aeronautics R&T Roundtable, Washington DC, 2016

[2] S.S. Kalsi, R.A. Badcock, J.G. Storey and K.A. Hamilton, "Motors employing REBCO CORC and MgB2 Superconductors for AC stator windings", IEEE Trans. on Applied Superconductivity, Vol. 31, No.9, December 2021

[3] P. Kshirsagar, "Superconducting Motor and Cryo-cooled Inverter Engine: SOARING", presented at ARPA-E Annual Program Review Meeting, June 28-30, 2022

[4] Balachandran, T., Lee, D., Salk, N. and Haran, K.S., "A fully superconducting air-core machine for aircraft propulsion", IOP Conference Series: Materials Science and Engineering (Vol. 756, No. 1, p. 012030). IOP Publishing, March 2020

[5] C.G. Cantemir, A. Munteanu and R. Jansen, "10 MW Ring Motor – OSU-NNX14AL87A", presented at Energy Tech 16, Wolstein Center, Cleveland, OH, Nov. 28-30, 2016

[6] R. Dorget, S. Ayat, R., A. Cipriani, J. Leveque, J. Labbe, T. Lubin, M. Sitko, J. Tanchon, and J. Lacapere, "Construction of a 250 kW Superconducting Flux Modulation Prototype for Aircraft Application', Presented at ASC22 in Honolulu 23-28, 2022

[7] Haran, K. S., Kalsi, S., Arndt, T., Karmaker, H., Badcock, R., Buckley, B., Haugan, T., Izumi, M., Loder, D., Bray, J. W., Masson, P., and Stautner, E. W., "High power density superconducting rotating machines—development status and technology roadmap," Superconductor Science and Technology, vol. 30, 2017, p. 123002. doi: 10.1088/1361-6668/aa833e

[8] Arndt, T., "High Temperature Superconductors (HTS) as Enabling Technology for Sustainable Mobility and Energy Efficiency", IEEE CSC & ESAS SUPERCONDUCTIVITY NEWS FORUM (global edition), February 2019. Plenary presentation 2PL1A-01 given at ASC 2018, October 28-November 02, 2018, Seattle, (USA).

[9] T. J. Haugan, "Properties of Ultra-Pure Aluminium Wires and Materials for Electric Power Components at Cryogenic Temperatures", Presented at the Cryogenic Engineering Conference – International Cryogenic Materials Conference (CEC-ICMC), 23 July 2021

[10] Felder J L, Brown G V, Kim H D and Chu J 2011 Turboelectric distributed propulsion in a hybrid wing body aircraft Proc. 20th Int. Society for Airbreathing Engines (Gothenburg, Sweden, 12–16 Sept. 2011)

[11] Kalsi, S.S., 2011. "Applications of high temperature superconductors to electric power equipment." John Wiley & Sons, ISBN 978-0-470-16768-7

[12] M.D. Sumption, J. Murphy, M. Susner and T. Haugan, "Performance metric of electrical conductors for aerospace cryogenic motors, generators, and transmission cables", Cryogenics, 111 (2020) 103171

[13] S.S. Kalsi, J.G. Storey, J.M. Brooks, G. Lumsden and R.A. Badcock, "Mechanical and electrical design of a synchronous superconducting aircraft motor", Paper # 4LPo1D-09 presented at the ASC-2022 in Honolulu, HI.

[14] Bumby, C. W., Badcock, R. A., Sung, H.-J., Kim, K.-M., Jiang, Z., Pantoja, A. E., Bernardo, P., Park, M., and Buckley, R. G., "Development of a brushless HTS exciter for a 10 kW HTS synchronous generator," Superconductor Science and Technology, vol. 29, 2016, p. 024008. doi: 10.1088/0953-2048/29/2/024008

[15] Hamilton, K., Pantoja, A. E., Storey, J. G., Jiang, Z., Badcock, R. A., & Bumby, C. W., "Asynchronous Magnet–Stator Topologies in a Squirrel-Cage Superconducting Dynamo," IEEE Transactions on Applied Superconductivity, Vol. 29(5), 2019 doi: 10.1109/TASC.2019.2892773

Acknowledgments
This work was supported by the New Zealand Ministry of Business, Innovation and Employment (MBIE) under Advanced Energy Technology Platforms contract no. RTVU2004.